Int. J. Heat Mass Transfer. Vol. 17, pp. 845–859. Pergamon Press 1974. Printed in Great Britain

PREDICTION OF FULLY-DEVELOPED FLOW IN A TUBE CONTAINING A TWISTED-TAPE

A. W. DATE*
Mechanical Engineering Department, Imperial College, London S.W.7

(*Received* 26 *November* 1973)

Abstract—The problem of fully-developed, laminar and turbulent, uniform-property flow in a tube containing a twisted-tape has been formulated in terms of partial differential equations of momentum and heat transfer. These equations have been solved by adapting an existing numerical procedure for two-dimensional elliptic equations to predict the friction and heat-transfer characteristics of the flow.

A set of laminar flow predictions are presented to demonstrate the influence of Reynolds number, twist-ratio, Prandtl number and the fin-parameter on the flow characteristics.

The turbulent-viscosity, necessary to predict the turbulent flow characteristics, has been calculated by solving differential equations for kinetic energy of turbulence and the energy dissipation rate. This approach is, however, found to be inadequate for accurate quantitative predictions; a measure for eliminating this inadequacy is suggested.

NOMENCLATURE

$a, b_1, b_2,$	coefficients in the general partial
$c, d,$	differential equation;
$C_N, C_S,$	coefficients in the general finite difference
$C_E, C_W,$	equation;
$C_p,$	specific heat;
$C_{\text{fin}},$	fin parameter;
$C_\mu, C_G, C_D,$	constants in the $k-\varepsilon$ turbulence model;
$D,$	diameter of the tube;
$D_h,$	hydraulic diameter;
$E,$	constant in the "log-law";
$f,$	friction factor based on hydraulic diameter;
$f_i,$	friction factor based on internal diameter;
$h,$	heat-transfer coefficient;
$H,$	pitch for 180° rotation of twisted-tape;
$k,$	kinetic energy of turbulence;
$K_f,$	thermal conductivity of fluid;
$K_m,$	thermal conductivity of tape metal;
$l,$	length scale of turbulence;
$n,$	distance between the wall grid node and the adjacent interior node;
$Nu,$	average Nusselt number based on hydraulic diameter;
$Nu_i,$	average Nusselt number based on internal diameter;
$P,$	pressure;
$\bar{P},$	mean pressure;
$P_0,$	variable pressure;
$Pr,$	Prandtl number;
$Pr_{\text{eff}},$	effective Prandtl number;
$q_r, q_\theta, q_z,$	heat fluxes, divided by C_p in radial, tangential and axial directions;
$Q,$	heat input per unit length;
$r_0,$	radius of the tube;
$r, \theta, z,$	cylindrical polar coordinates;
$r', \theta', z',$	coordinates of a rotating coordinate system;
$Re,$	Reynolds number based on hydraulic diameter;
$Re_i,$	Reynolds number based on internal diameter;
$S,$	source term of finite-difference equation;
$s,$	distance from the wall;
$T,$	temperature;
$V_r, V_\theta, V_z,$	radial, tangential and axial time–mean velocity;
$V_\tau,$	shear velocity;
$y,$	twist ratio.

Greek letters

$\delta,$	thickness of the twisted tape;
$\varepsilon,$	dissipation;
$\mu,$	dynamic viscosity;
$\mu_{\text{eff}},$	effective viscosity;
$\rho,$	density;
$\phi,$	dependent variable of the partial differential equation;
$\psi,$	stream function;
$\Gamma,$	laminar diffusivity multiplied by ρ;
$\Gamma_{\text{eff}},$	effective value of Γ;

*Present address: Department of Mechanical Engineering, Indian Institute of Technology, Bombay-400076.

ω, axial vorticity;
κ, constant in the "log-law".

Subscripts

b, bulk value over the cross-section;
m, mean value over the cross-section;
0, wall grid node;
no, near-wall grid node;
turb, turbulent part of the effective value;
eff, effective value.

1. INTRODUCTION

TWISTED-TAPE inserts inside circular tubes provide a means of increasing the surface heat-transfer coefficient within the tubes of tubular heat exchangers. Figure 1 shows the layout of a tube containing a twisted-tape. The tape consists of a long metal strip which has been twisted about its longitudinal axis, the width of the tape being equal to the internal diameter of the tube.

The pressure-drop and heat-transfer characteristics of the fully-developed turbulent flow in tubes containing twisted tapes have been investigated experimentally by many investigators (see, for example, [1–3]); and empirical correlations to predict these characteristics have been proposed. A survey carried out by the present author (see Date [18]) showed that the available experimental data are not extensive, and the correlations to predict them are applicable only for a certain range of the values of the independent parameters. For example, no experimental data exist for laminar flows, and for fluids with high Prandtl numbers. Similarly, the proposed correlations do not demonstrate consistent agreement regarding, for example, the influence of fluid-property variations or Prandtl number on Nusselt numbers. In order to gain knowledge of the characteristics of the flow over a range of conditions, more experimental data are needed. However, the effort involved will be prohibitively expensive.

A less time-and-cost-consuming approach is to derive and solve the differential equations which describe the transport of momentum and heat in the twisted tape flow. The purpose of the present paper is firstly, to show how the necessary transport equations are derived, and solved numerically on a computer; and secondly, to present predicted characteristics of the flow to demonstrate the scope of the numerical procedure described in the paper. Of course, the numerical procedures do not eliminate the need for experiments, but they certainly diminish their extent and cost by highlighting the most influential parameters governing the characteristics under given conditions.

The paper is divided into further four sections: Section 2 describes the derivation of the necessary transport equations; Section 3 shows how an existing numerical procedure is adapted to solve the equations; in Section 4, some predicted data are presented; and finally, concluding remarks are made in Section 5.

2. THE MATHEMATICAL PROBLEM

2.1. *The domain of interest*

In the region of the fully-developed flow, the distributions of the velocities are independent of the axial distance along the tube; in other words, they are identical at every cross-section of the tube. One such cross-section is shown in Fig. 1 (section A–A).

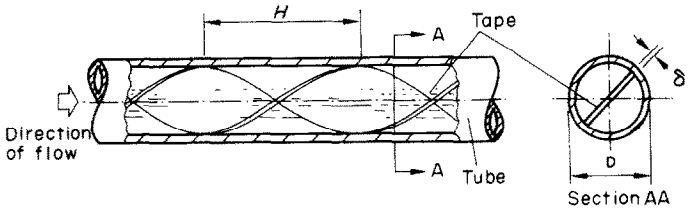

FIG. 1. Illustration of the twisted-tape inside a circular tube.

Contrary to the real situation, it is assumed here that the width of the tape exactly equals the internal diameter of the tube. The ratio of the tape thickness δ to the tube diameter D is usually small for the free space to be regarded as two twisting ducts of semi-circular cross-section which rotate through 180 degrees in an axial distance H. Since the flow will be identical in each of the two semi-circular sections, only one of these need be considered.

2.2. *The coordinate system*

The only suitable coordinate system is one in which the angular coordinate is measured always from the surface of the twisted-tape. Such a rotating cylindrical polar coordinate system (r', z', θ') say (see Fig. 2), is then related to the customary stationary system (r, z, θ) by the following equations:

$$r' = r,$$
$$z' = z, \qquad (1)$$
$$\text{and} \quad \theta' = \theta + \pi z/H.$$

The positive sign before $\pi z/H$ implies anti-clockwise rotation of the tape as z increases, when distances z' and z are measured in the direction of axial flow, and θ and θ' are measured in the clockwise direction.

As a consequence of equations (1), the following relations may be written:

$$\frac{\partial}{\partial r} = \frac{\partial}{\partial r'}, \quad \frac{\partial}{\partial \theta} = \frac{\partial}{\partial \theta'}, \quad \text{and} \quad \frac{\partial}{\partial z} = \frac{\partial}{\partial z'} + \frac{\pi}{H}\frac{\partial}{\partial \theta'}. \tag{2}$$

These relations are now employed to transform the well-established (see Bird *et al.* [4]) transport equations of momentum and heat in (r, z, θ) system to those in (r', z', θ') system.

2.3. *The transport equations in* (r', z', θ') *system*

The starting point in the derivation of the necessary transport equations is the equations in the (r, z, θ) system. Before making use of these equations, the following mathematical condition of the fully-developed flow must be noted. It is that,

$$\frac{\partial}{\partial z'} = 0, \tag{3}$$

for all dependent variables, except for the mean pressure $\bar{P}$, and temperature T, and $\partial\bar{P}/\partial z'$ and $\partial T/\partial z'$ are to be treated as known constants.

It follows from equations (2) and (3) that the continuity, momentum and heat transport equations in (r', z', θ') system are as follows:

Continuity equation

$$\rho\left\{\frac{1}{r'}\frac{\partial(r'V_r)}{\partial r'} + \frac{1}{r'}\frac{\partial}{\partial\theta'}\left(V_\theta + \frac{\pi r'}{H}V_z\right)\right\} = 0, \tag{4}$$

Axial momentum equation

$$\rho\left\{V_r\frac{\partial V_z}{\partial r'} + \left(\frac{V_\theta}{r'} + \frac{\pi}{H}V_z\right)\frac{\partial V_z}{\partial\theta'}\right\} = -\left\{\frac{\partial\bar{P}}{\partial z'} + \frac{\pi}{H}\frac{\partial P_0}{\partial\theta'}\right\} - \left\{\frac{1}{r'}\frac{\partial}{\partial r'}(r'\tau_{r,z}) + \frac{1}{r'}\frac{\partial}{\partial\theta'}(\tau_{\theta,z}) + \frac{\pi}{H}\frac{\partial}{\partial\theta'}(\tau_{zz})\right\}, \tag{5}$$

Tangential momentum equation

$$\rho\left\{V_r\frac{\partial V_\theta}{\partial r'} + \left(\frac{V_\theta}{r'} + \frac{\pi V_z}{H}\right)\frac{\partial V_\theta}{\partial\theta'} + \frac{V_r V_\theta}{r'}\right\} = -\frac{1}{r'}\frac{\partial P_0}{\partial\theta'} - \left\{\frac{1}{r'^2}\frac{\partial}{\partial r'}(r'^2\tau_{r,\theta}) + \frac{1}{r'}\frac{\partial(\tau_{\theta,\theta})}{\partial\theta'} + \frac{\pi}{H}\frac{\partial(\tau_{\theta,z})}{\partial\theta'}\right\}, \tag{6}$$

Radial momentum equation

$$\rho\left\{V_r\frac{\partial V_r}{\partial r'} + \left(\frac{V_\theta}{r'} + \frac{\pi}{H}V_z\right)\frac{\partial V_r}{\partial\theta'} - \frac{V_\theta^2}{r'}\right\} = -\frac{\partial P_0}{\partial r'} - \left\{\frac{1}{r'}\frac{\partial(r'\tau_{r,r})}{\partial r'} + \frac{1}{r'}\frac{\partial\tau_{r,\theta}}{\partial\theta'} - \frac{\tau_{\theta,\theta}}{r'} + \frac{\pi}{H}\frac{\partial\tau_{r,z}}{\partial\theta'}\right\}, \tag{7}$$

Temperature equation

$$\rho\left\{V_r\frac{\partial T}{\partial r'} + \left(\frac{V_\theta}{r'} + \frac{\pi}{H}V_z\right)\frac{\partial T}{\partial\theta'}\right\} = -\rho V_z\frac{\partial T}{\partial z'} - \left\{\frac{1}{r'}\frac{\partial}{\partial r'}(r'q_r) + \frac{1}{r'}\frac{\partial(q_\theta)}{\partial\theta'} - \frac{\pi}{H}\frac{\partial(q_z)}{\partial\theta'}\right\}. \tag{8}$$

Since $\partial\bar{P}/\partial z'$ and $\partial T/\partial z'$ are known constants, equations (4–8) are two-dimensional: the dependent variables, V_z, V_θ, V_r and T, that were functions of r, z and θ are now functions of r' and θ' alone. These equations are general, and applicable to both laminar and turbulent flows if, in the latter case, the instantaneous velocities are replaced by their time-averaged values.

It is important, at this stage, to note the way in which the pressure-terms in equations (4–7) are treated. It is assumed that the pressure at any point in the flow consists of two parts. Thus, P is expressed as:

$$P(r, z, \theta) = \bar{P}(z') + P_0(r', \theta') \tag{9}$$

where $\bar{P}(z')$ is the mean pressure at a cross-section and $P_0(r', \theta')$ is that component of the pressure which varies over the cross-section.

The terms on the left hand side of the equations (5)–(8) represent the convective fluxes, whereas the terms containing τ's and q's represent the diffusive fluxes of momentum and heat respectively. When information regarding τ's and q's is specified, the mathematical statement of the transport equations is complete.

2.4. *The diffusion fluxes*

For laminar fluids, the stresses τ's are related* to the velocity gradients (or strain) via μ. Similarly, q's are related* to the temperature gradients via Γ; and μ and Γ are constants for uniform property fluids. For turbulent flow one may postulate the existence of *effective* exchange coefficients analogous to μ and Γ. Thus, for turbulent flow,

$$\text{and} \quad \left.\begin{aligned}\mu_{\text{eff}} &= \mu + \mu_{\text{turb}},\\ \Gamma_{\text{eff}} &= \Gamma + \Gamma_{\text{turb}}\end{aligned}\right\}. \tag{10}$$

The subscript "turb" signifies the turbulent part of the effective values. Further, it may be postulated that:

$$\Gamma_{\text{eff}} = \mu_{\text{eff}}/Pr_{\text{eff},T}, \tag{11}$$

*The relations for each stress and heat flux component in a rotating coordinate system are given in Date [19].

where $Pr_{\text{eff},T}$ if the effective Prandtl number. Experimental evidence (see Spalding [5]) suggests that its value is about 0·9.

Thus the τ's and q's are replaced by one unknown μ_{eff}; in Section 2.7, the method adopted for its determination is discussed. For the time being it is assumed that μ_{eff} is knowable.

In the discussion to follow, use will be made of equations (10) and (11) to represent the diffusion fluxes, with a reminder that when laminar flow is considered, μ_{eff} and $Pr_{\text{eff},T}$ are to be replaced by the respective laminar values: the laminar viscosity μ and the laminar Prandtl number Pr.

2.5. *Introduction of vorticity and stream function*

Equations (5)–(8), after substituting expressions for τ's and q's, form a set of equations which need to be solved. From the point of view of numerical solutions, the explicit appearance of pressure P_0 in these equations poses certain difficulties. To eliminate its appearance from equations (6) and (7), the axial vorticity ω is introduced such that the information contained in the two equations is completely described by a single equation for ω, where ω is defined as:

$$\omega = \frac{1}{r'}\left\{\frac{\partial V_r}{\partial \theta'} - \frac{\partial (r' V_\theta)}{\partial r'}\right\}. \tag{12}$$

The process of arriving at the vorticity equation is as follows: differentiate equations (6) with respect to r', and equation (7) with respect to θ', and subtract the first from the second. Using the definition (12), the resulting expression can be transformed into the required vorticity equation. It is as follows:

The vorticity equation

$$\rho\left\{V_r \frac{\partial \omega}{\partial r'} + \left(\frac{V_\theta}{r'} + \frac{\pi}{H} V_z\right)\frac{\partial \omega}{\partial \theta'}\right\} =$$

$$-\left\{\frac{1}{r'}\frac{\partial}{\partial r'}\left(r' \frac{\partial}{\partial r'}(\mu_{\text{eff}} \cdot \omega)\right) + \left(\frac{1}{r'^2} + \frac{\pi^2}{H^2}\right)\frac{\partial}{\partial \theta'}\left(\frac{\partial (\mu_{\text{eff}} \cdot \omega)}{\partial \theta'}\right)\right\}$$

$$+\rho \frac{\pi}{H}\left\{\frac{1}{r'}\frac{\partial V_z}{\partial r'}\frac{\partial (r' V_\theta)}{\partial r'} - \frac{\partial V_z}{\partial r'}\frac{\partial V_\theta}{\partial \theta'}\right\} + S_\omega$$

where (13)

$$S_\omega = \frac{1}{r'}\frac{\partial^2}{\partial \theta'^2}\left\{\mu_{\text{eff}}\left(\frac{\partial V_\theta}{\partial r'} - \frac{V_\theta}{r'}\right)\right\} - \frac{\partial}{\partial r'}\left\{r' \frac{\partial}{\partial r'}\left(\mu_{\text{eff}} \frac{\partial V_r}{\partial \theta'}\right)\right\}$$

$$-2\frac{\partial^2}{\partial r'^2}\left(V_\theta \frac{\partial \mu_{\text{eff}}}{\partial r'}\right) + \frac{\partial^2}{\partial r' \partial \theta'}\left(\mu_{\text{eff}} \frac{\partial V_r}{\partial \theta'}\right)$$

$$+\frac{\partial}{\partial \theta'}\left\{\mu_{\text{eff}} \frac{\partial (V_r/r')}{\partial r'}\right\} + \frac{\partial^2}{\partial r' \partial \theta'}\left\{\mu_{\text{eff}}\left(\frac{1}{r'}\frac{\partial V_\theta}{\partial \theta'} + \frac{2V_r}{r'}\right)\right\}$$

$$+\frac{\pi}{H}\left\{\frac{\partial^2}{\partial \theta'^2}\left(\mu_{\text{eff}} \frac{\partial V_z}{\partial r'}\right) + \frac{\partial^2}{\partial r' \partial \theta'}\left(\mu_{\text{eff}} \frac{\partial V_z}{\partial \theta'}\right)\right\}.$$

The appearance of P_0 from equation (5) for axial momentum is still not removed, although it is easily seen that the term $\partial P_0/\partial \theta'$ can be found from equation (6).

Now the stream function ψ is defined thus:

$$\frac{\partial \psi}{\partial r'} = \rho\left(V_\theta + \frac{\pi r'}{H} V_z\right), \tag{14}$$

and

$$\frac{\partial \psi}{\partial \theta'} = -\rho r' V_r. \tag{15}$$

These definitions, along with the definition of vorticity can be manipulated so that, the statement of mass conservation, as expressed by the continuity equation (4), is implicitly satisfied. The result of this manipulation is generally termed as the stream function equation:

The stream function equation

$$\left\{\frac{1}{r'}\frac{\partial}{\partial r'}\left(r' \frac{\partial \psi}{\partial r'}\right) + \frac{1}{r'^2}\frac{\partial^2 \psi}{\partial \theta'^2}\right\}$$

$$+\rho\left\{\omega - \frac{\pi}{Hr'}\frac{\partial (V_z r'^2)}{\partial r'}\right\} = 0. \tag{16}$$

Thus, by introducing ω and ψ the mathematical statement of the problem has been redefined; but with the following advantages:

1. Since the stream function equation satisfies mass conservation, no explicit recourse to the continuity equation is necessary.
2. The introduction of ω has replaced equations (6) and (7) by a single equation for ω; at the same time, partial elimination of pressure P_0 has also been achieved.

The equations, which now need to be solved are: equation (16) for ψ, equation (13) for ω, equation (5) for V_z and equation (8) for T.

Following Gosman *et al.* [6] these equations can be represented in a general form.

2.6. *Generalized representation of the equations*

The terms

$$\left(\frac{V_\theta}{r'} + \frac{\pi}{H} V_z\right) \quad \text{and} \quad V_r$$

appear as multipliers on the left-hand side of the equations for ω, V_z and T. These terms can be replaced by stream function via equations (14) and (15). This done, the equations for ψ, ω, V_z and T can be represented by a general equation for any dependent-

Table 1. Equations for ψ, ω, V_z and T

ϕ	a	b_1	b_1	c	d
ψ	0	$1/\rho r'$	r'/ρ	1	$r'\left\{\frac{\pi}{H}\frac{1}{r'}\frac{\partial(V_z r'^2)}{\partial r'}-\omega\right\}$
ω	1	$\left(\frac{1}{r'}+\frac{\pi^2 r'}{H^2}\right)$	r'	μ_{eff}	d_ω^*
V_z	1	$\mu_{\text{eff}}\left(\frac{1}{r'}+\frac{\pi^2 r'}{H^2}\right)$	$\mu_{\text{eff}} r'$	1	$r'\left\{\frac{\partial \bar{P}}{\partial z'}+\frac{\pi}{H}\frac{\partial P_0}{\partial \theta'}\right\}$
T	1	$\Gamma_{\text{eff},T}\left(\frac{1}{r'}+\frac{\pi^2 r'}{H^2}\right)$	$\Gamma_{\text{eff},T} r'$	1	$-r' V_z \frac{\partial T}{\partial z'}$

*The term d_ω is as follows:

$$d_\omega = \frac{\pi r'}{H}\left[\frac{\partial V_z}{\partial \theta'}\left\{\frac{1}{r'}\frac{\partial}{\partial r'}\left(r'\frac{\partial \psi}{\partial r'}\right)-\frac{\rho \pi r'}{H}\frac{\partial}{\partial r'}(V_z r'^2)\right\}-\frac{\partial V_z}{\partial r'}\left\{\frac{\partial^2 \psi}{\partial r' \partial \theta'}-\frac{\rho \pi r'}{H}\frac{\partial V_z}{\partial \theta'}\right\}\right]+S_\omega$$

variable ϕ. This general equation is as follows:

$$\underbrace{a\left\{\frac{\partial}{\partial \theta'}\left(\phi\frac{\partial \psi}{\partial r'}\right)-\frac{\partial}{\partial r'}\left(\phi\frac{\partial \psi}{\partial r'}\right)\right\}}_{\text{convection terms}}-\underbrace{\frac{\partial}{\partial \theta'}\left\{b_1\frac{\partial(c\phi)}{\partial \theta'}\right\}-\frac{\partial}{\partial r'}\left\{b_2\frac{\partial(c\phi)}{\partial r'}\right\}}_{\text{diffusion terms}}+\underbrace{d=0,}_{\text{source terms}} \tag{17}$$

where expressions for a, b_1, b_2, c and d for each dependent variable ϕ are given in Table 1.

Such a generalized representation of the equations will allow concentration on equation (17), when the numerical solution of the equations is discussed in Section 3. Before proceeding to Section 3, however, here is a reminder: A method for determining μ_{eff}, which is vital to the prediction of turbulent flow is still not described. Determination of μ_{eff} is the subject matter of the next sub-section.

2.7. *Determination of μ_{eff} for turbulent flow*

To determine μ_{eff}, one must determine the spatial distribution of μ_{turb} over the semi-circular cross-section. One may specify μ_{turb} as an external information to the set of equations, or it may be related to the product of (Prandtl's) mixing length and the local velocity gradient, where the mixing length is again specified by an algebraic expression. However, since the twisted-tape flow is assymetric, the algebraic expressions, referred to above, are difficult to invent, especially in the absence of extensive experimental data for velocity profiles.

Here, a method is chosen which does not necessitate specification of any algebraic expressions; but simply requires specification of certain constants which may be universal. The method is as follows:

Following the dimensional arguments of Prandtl [9] and Kolmogorov [8] μ_{turb} is written as:

$$\mu_{\text{turb}} = C_\mu \rho k^2/\varepsilon \tag{18}$$

where k is the kinetic energy of turbulence, and ε is the energy dissipation rate; C_μ is a constant whose value is to be specified. Now, the spatial distributions of k and ε are determined by solving, with appropriate boundary conditions, the partial differential equations for the conservation of k and ε. The complete description of the derivation of these equations is beyond the scope of this paper; here their final forms are presented in the same manner as those for ψ, ω, V_z and T in Table 1.

Table 2. Equations for k and ε

ϕ	a	$b1$	$b2$	c	d
k	1	$\Gamma_{\text{eff},k}\left(\frac{1}{r'}+\frac{\pi^2 r'}{H^2}\right)$	$\Gamma_{\text{eff},k} r'$	1	$r'(G-\rho\varepsilon)$
ε	1	$\Gamma_{\text{eff},\varepsilon}\left(\frac{1}{r'}+\frac{\pi^2 r'}{H^2}\right)$	$\Gamma_{\text{eff},\varepsilon} r'$	1	$r'\left(C_G\frac{\varepsilon}{k}G-C_D\rho\varepsilon^2/k\right)$

where

$$\text{and} \qquad \begin{aligned}\Gamma_{\text{eff},k} &= \mu_{\text{eff}}/Pr_{\text{eff},k},\\ \Gamma_{\text{eff},\varepsilon} &= \mu_{\text{eff}}/Pr_{\text{eff},\varepsilon};\end{aligned} \tag{19}$$

and $Pr_{\text{eff},k}$ and $Pr_{\text{eff},\varepsilon}$, like $Pr_{\text{eff},T}$ are constants. C_G and C_D are other two constants; and G, which stands for the generation of kinetic energy, is given by:

$$G = \mu_{\text{turb}}\left[2\left\{\left(\frac{\partial V_r}{\partial r'}\right)^2+\frac{\pi^2}{H^2}\left(\frac{\partial V_z}{\partial \theta'}\right)^2+\frac{1}{r'^2}\left(\frac{\partial V_\theta}{\partial \theta'}+V_r\right)^2\right\}+\left\{\left(\frac{\partial V_\theta}{\partial r'}-\frac{V_\theta}{r'}+\frac{\partial V_r}{\partial \theta'}\right)^2+\left(\frac{\partial V_z}{\partial r'}+\frac{\pi}{H}\frac{\partial V_r}{\partial \theta'}\right)^2+\frac{1}{r'^2}\left(\frac{\pi}{H}\frac{\partial V_\theta}{\partial \theta'}+\frac{\partial V_z}{\partial \theta'}\right)^2\right\}\right]. \tag{20}$$

Jones and Launder [10] have suggested the following values for the various constants mentioned in the above discussion:

$$C_\mu = 0{\cdot}09,$$
$$C_G = 1{\cdot}55,$$
$$C_D = 2{\cdot}0, \qquad (21)$$
$$Pr_{\text{eff},k} = 1{\cdot}0,$$
and $$Pr_{\text{eff},\varepsilon} = 1{\cdot}3.$$

Note that $Pr_{\text{eff},T}$ equals 0·9 (see equation 11).

These values of the constants have proved to be valid in many flow situations. For example, Laufer's [20] experimentally measured axial velocity profiles for fully-developed flow in a circular pipe can be predicted within 1 per cent (see Date [19]); the performance of two-dimensional film-cooling geometries was predicted accurately by Mathews [11].

The numerical procedure to be described in the next section is applicable to the equations of k and ε as well; here it is emphasized again that these equations have eliminated the need for algebraic specification of μ_{turb}. The extent of the success of this method will be demonstrated in Section 4, where some typical predictions are presented.

2.8. *Closure*

The set of differential equations specified above cannot be solved unless the conditions of the variables ϕ are specified on the boundaries. The boundaries of interest are: the tube wall surface and the twisted-tape surface at any semi-circular cross-section. The discussion of the boundary conditions is deferred to the next section for convenience.

3. THE NUMERICAL SOLUTION OF THE EQUATIONS

3.1. *The finite-difference equations and their solution*

The finite-difference solution procedure adopted to solve the general partial differential equation (17) is described in detail by Gosman *et al.* [6]; therefore, only its main features are described here.

Essentially, the partial differential equation (17) for each variable ϕ (4 variables for laminar flow and 6 variables for turbulent flow) is converted into a set of algebraic equations through a finite-difference algorithm. These algebraic equations can be formulated as follows*:

$$\phi_p = C_N \phi_N + C_S \phi_S + C_E \phi_E + C_W \phi_W + S, \qquad (22)$$

where the C's are the coefficients which usually depend on the variables ϕ's, and depending on the influence of convective and diffusive fluxes, determine how heavily the neighbouring values of ϕ should weigh in the determinations of ϕ_p. The effects of sources of ϕ are contained in term S.

*See Fig. 2 for the meaning of the subscripts.

There is one such equation for each variable ϕ at every interior node of the grid; with conditions specified on the boundaries (node referred to by 0 in Fig. 2), there will be as many equations as there are unknowns. The set of algebraic equations given by (22), therefore, is a solvable set. The solution of this set, however, will require an iterative procedure because the C's and S depend on the ϕ's. Gosman *et al.* adopt the Gauss–Seidel iteration procedure which incorporates the successive substitution formula.

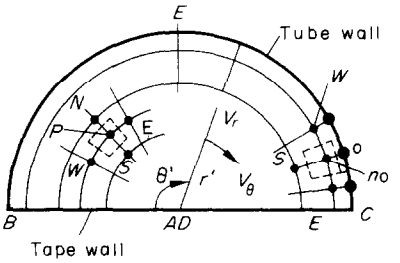

FIG. 2. Illustration of the grid-distribution, and a typical interior node P of the grid. Note the area called "cell" bounded by dotted lines, and the wall node (0) and the near-wall node (no).

For the twisted-tape flow equations described in Section 2, this standard iteration procedure does not always produce convergence. For instance, in computations at very high Reynolds numbers and high twists of the tape, the source term of the vorticity equation (see Table 1) becomes very large. Under these conditions, a given flow perturbation (i.e. a change in ψ and V_z) produces a large change in ω_p (see equation 22). This change in ω_p causes the stream function to be altered greatly, since ω_p appears in the source term of the stream function equation. This greatly altered stream function distribution perturbs the flow further. Clearly this computation scheme can become unstable, although the physical flow situation is a stable one. Gosman and Spalding [7] suggested an iterative procedure to cure such an instability; the procedure was called the "Multi-point circulation adjustment" (MPCA) procedure. The application of the procedure to the twisted-tape flow equations is described in detail in Date [19]; here, only its principal features are summarized.

The procedure simultaneously adjusts the value of vorticity ω_p and its neighbours ω_N, ω_S, ω_E and ω_W, and subsequently the stream function ψ_p in a single sweep of the field of computation. The constraints on these adjustments are:

(a) that the imbalance in equation (22) for vorticity is reduced to zero at every grid node;
(b) that the "circulation principle" for the cells surrounding grid nodes P, N, S, E and W is satisfied.

The circulation principle requires that:

$$\int_A \omega . \mathrm{d}A = \oint V . \mathrm{d}S \tag{23}$$

where A is area of the cell, V is the velocity along the boundaries of the cell, and $\mathrm{d}S$ is the incremental length along these boundaries.

Besides MPCA, there are other conventional procedures such as the under-relaxation of the finite-difference equations and the under-relaxation of source terms of the equations which are necessary to obtain convergence; the details of these are given in Date [19].

3.2. *Boundary conditions*

As mentioned in the previous section, boundary conditions are necessary to "close" the numerical problem. The equations for fully-developed flow are two-dimensional and elliptic, and conditions of the variables ϕ must be specified on four boundaries of the domain of interest. These boundaries, with reference to Fig. 2, are: *AB*, *BEC*, *CD*, and *DA*. The boundary *DA* is essentially the centre point of the twisted-tape; here it is treated as a boundary of zero radius.

In the subsequent discussion the boundary conditions for the laminar and turbulent flow are described separately.

Laminar flow. Each boundary of the domain of interest represents a solid wall; the velocity V_z is therefore zero on all boundaries, and the stream function ψ assumes a constant value: ψ was assigned the value zero in the present calculations. The values of ω and T, however, require further consideration.

Vorticity is defined in terms of the gradients of the cross-stream velocities but the distribution of these velocities in the near-wall region is unknown. The boundary conditions for vorticity can however be obtained from the "no-slip" condition, and from the assumption regarding the profiles of the velocity components in the near-wall region. The complete derivation of the boundary conditions can be found in Date [19]; here, it will suffice to note the general form of the boundary conditions appropriate to the four boundaries. It is as follows:

$$\omega_0 = g_1 \frac{(\psi_0 - \psi_{\mathrm{no}})}{\rho n^2} + g_2 \omega_{\mathrm{no}} + g_3 V_{z,\mathrm{no}} \tag{24}$$

where subscripts 0 and no refer to the boundary node and to the adjacent interior one respectively; n denotes the distance between the two nodes (see Fig. 2 for illustration); and g_1, g_2, g_3 are dimensionless numbers.

In the present calculations it is assumed that the temperature on the tube wall *BEC* is maintained at a uniform value. The temperature on the tape surface, i.e. the boundaries *AB*, *CD*, and *DA*, is unknown. It can be determined by referring to the fin-action of the twisted-tape, and by solving a one-dimensional heat-conduction equation along the width of the tape. Here the result of the analysis which is given in Date [19] is presented. The analysis gives rise to a quadratic expression for the tape surface temperature T_0, say; this expression is:

$$aT_0^2 + bT_0 + c = 0, \tag{25}$$

where a, b and c are functions of the temperatures at nodes adjacent to T_0, and C_{fin}, where C_{fin} is the fin-parameter defined as:

$$C_{\mathrm{fin}} = \frac{k_m}{k_f} \frac{\delta}{D}. \tag{26}$$

Turbulent flow. In the close vicinity of the wall, dependent variables such as V_z, k, ω, T, etc., for turbulent flow, vary rapidly with distance from the wall. Therefore, to preserve the accuracy of the finite difference procedure, very fine grids will be necessary in this region. Consequently, the computer time will increase substantially.

To obviate this shortcoming, implications of the "log-law of the wall" suggested by Backshall and Landis [17] are used to serve as the boundary conditions. The suggested law pertains to the representation of the variation of the axial (V_z) and the cross-stream* (V_{cs}) velocities in the near-wall region with the distance from the wall. The complete derivation of the boundary conditions is given in Date [19], here the suggested log-law and the boundary conditions are stated.

$$V_{cs} = \frac{V_{cs,\tau}}{\kappa} \sqrt{\cos\alpha} \ln\left(\frac{E s V_{cs,\tau} \rho}{\mu \sqrt{\cos\alpha}}\right) \tag{27}$$

and

$$V_z = \frac{V_{z,\tau}}{\kappa} \sqrt{\sin\alpha} \ln\left(\frac{E s V_{z,\tau} \rho}{\mu \sqrt{\sin\alpha}}\right) \tag{28}$$

where α is the angle between the direction of the absolute velocity and the cross-sectional plane and $V_{cs,\tau}$ and $V_{z,\tau}$ are the cross-stream and axial shear velocities respectively.

With reference to Fig. 2, the boundary conditions are as follows:

$$\psi_0 = 0, \tag{29}$$

$$V_{z,0} = V_{z,\mathrm{no}} - \frac{V_{z,\tau}\sqrt{\sin\alpha}}{\kappa}, \tag{30}$$

$$\omega_{\mathrm{no}} = \frac{V_{cs,\tau}}{n} \sqrt{\cos\alpha}, \tag{31}$$

$$K_{\mathrm{no}} = C_\mu^{-1/2} V_\tau^2, \tag{32}$$

*V_{cs} refers to V_θ near the tube-wall; it refers to $V_r \cos\theta_1'$ near the tape-wall, θ_1' being the angle made by the first radial grid-line away from the tape-wall with the tape-wall.

and

$$\varepsilon_{no} = \frac{\rho V_\tau^3}{n}, \tag{33}$$

where

$$V_\tau = \frac{V_{z,\tau}}{\sqrt{\sin\alpha}} = \frac{V_{cs,\tau}}{\sqrt{\cos\alpha}}, \tag{34}$$

and

$$\alpha = \tan^{-1}\left(\frac{V_{z,no}}{V_{cs,no}}\right) \tag{35}$$

In equation (35), $V_{cs,no}$ is evaluated from the definition of stream function and the log-law of the wall; and $V_{cs,\tau}$ and $V_{z,\tau}$ in equations (30) and (31) are calculated by iterating equations (27) and (28) with $V_z = V_{z,no}$, $V_{cs} = V_{cs,no}$ and $s = n$, all of which are known. Thus it is seen that the variables ω, k and ε are specified at the first grid-node away from the wall whereas ψ and V_z are specified at the wall, $V_{z,0}$ being the slip velocity deliberately introduced (see, Patankar and Spalding [26]).

To account for the steep gradients of temperature near a wall, the value of Γ_{eff} at the grid-node no is calculated from the law suggested by Spalding and Jayatillake [25]; the details of calculations can be found in Date [19].

4. PRESENTATION AND DISCUSSION OF RESULTS

4.1. *Laminar flow*

4.1.1. *Method of prediction.* To predict the friction characteristics, the equations of ψ, ω, and V_z were solved for given input values of μ, ρ, $\partial\bar{P}/\partial z'$ and π/H. The predicted profile of V_z enables the calculation of Reynolds number Re_i and the friction factor f_i. Thus:

$$f_i = \frac{1}{2}\frac{\partial\bar{P}}{\partial z'}\frac{D}{\rho V_{z,m}^2}; \tag{36}$$

and

$$Re_i = \frac{\rho V_{z,m} D}{\mu}; \tag{37}$$

where $V_{z,m}$ is the mean value of V_z.

The predicted distribution of V_z and ψ is subsequently used to solve the temperature equation. This requires additional inputs, which are: the Prandtl number Pr, and the fin-parameter C_{fin}, and the source term $\partial T/\partial z'$. In solving the temperature equation, a dimensionless temperature T^* is used, where:

$$T^* = (T - T_w)/(Q/k_f), \tag{38}$$

where Q is the uniform heat flux per unit axial distance. The $\partial T^*/\partial z'$ can then be determined from the overall heat balance over a length $\Delta z'$ as:

$$\frac{\partial T^*}{\partial z'} = \frac{4}{\pi r_0 Re_i Pr}. \tag{39}$$

$\partial T^*/\partial z'$ is now a known constant since Re_i and Pr are known.

The predicted value of T^*, and its mean value T_b^* enables evaluation of the average Nusselt number Nu_i. Thus:

$$Nu_i = \frac{hD}{k_f}, \tag{40}$$

where,

$$h = Q/(T_w - T_b)/\pi D, \tag{41}$$

and, therefore,

$$Nu_i = -1/T_b^*/\pi. \tag{42}$$

The evaluation of the mean values of V_z and T^* in the above calculations is carried out by using Simpson rule.

The predictions to be presented were obtained with 15×15 uniformly-spaced grids. This grid size provided sufficient numerical accuracy (see Date [19]).

4.1.2. *Friction characteristics.* Figure 3 shows the predicted variation of f_i with Re_i at different values of y. The solid line for $y = \infty$ corresponds to the flow in a straight semi-circular duct for which an analytical solution is available (Weigand [12]). The present prediction agreed with this exact solution within 1 per cent.

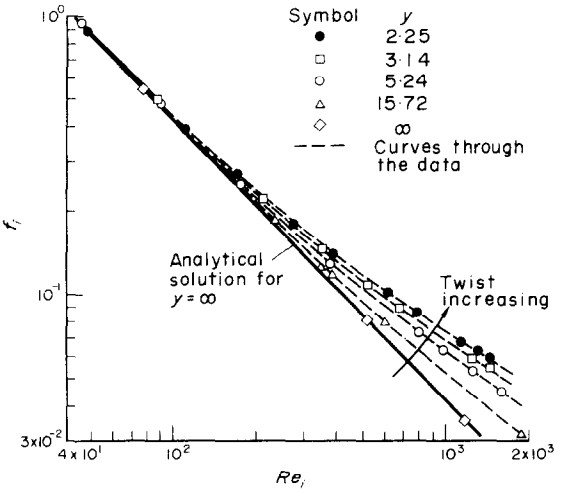

FIG. 3. Predicted friction factor data for fully-developed laminar flow.

The predicted data which lie above this line correspond to those cases in which the tape possesses a finite twist. As would be expected, for the same flow rate (or same Re_i), the friction factor increases as y decreases. Also at lower Reynolds numbers the data converge on the line for $y = \infty$, irrespective of the value of y. Thus the friction factor data show plausible trends.

Figure 4 shows the effect of y on the predicted axial velocity profiles as $Re_i \approx 1200$. The effect of twist is evident from the assymetry exhibited by the profiles. As the twist increases (or y decreases), the profiles disintegrate into a pattern which shows two peaks of axial velocity.

It should be noted here that unlike in the case of $y = \infty$, secondary flow exists in cases for which $y < \infty$. The magnitude of the secondary velocities increases with increase in Re_i and decrease in y. In the present friction factor data, converge on the line for $y = \infty$.

Effect of Prandtl number on Nusselt number at $C_{fin} = \infty$—Figure 6 shows the variation of Nu_i with Re_i for various Prandtl numbers. The solid horizontal line again corresponds to the case of $y = \infty$; as would be expected, the predicted value of Nu_i is unaltered by the value of Prandtl number.

The predicted curves which lie above the solid line represent predictions for $y = 5{\cdot}24$, and they signify the fact that for $y < \infty$, when secondary flow exists, the

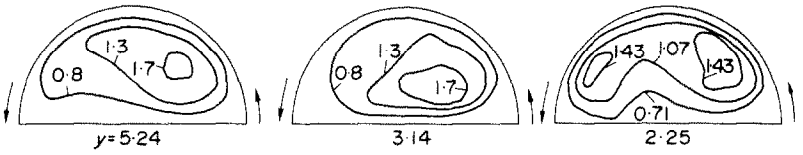

FIG. 4. Effect of twist-ratio on predicted profiles of axial velocity ($V_z/V_{z,m}$) at $Re_i \approx 1200$ (arrows indicate rotation of tape in the direction of flow).

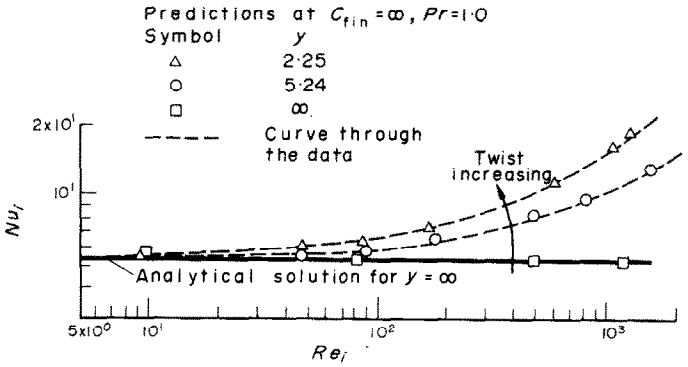

FIG. 5. Influence of twist-ratio on Nusselt number at $C_{fin} = \infty$

predictions, the mean values of the secondary velocity

$$V_{cs}\left(=\sqrt{V_r^2+V_\theta^2}\right)$$

were found to be between 10 and 35 per cent of the mean axial velocity.

4.1.3. *Heat-transfer characteristics. Effect of twist-ratio on Nusselt number at* $C_{fin} = \infty$—Figure 5 shows the variation of Nu_i with Re_i for various values of y for maximum fin-effect. The solid horizontal line corresponds to the analytical solution for $y = \infty$ (Eckert *et al.* [13]); and represents $Nu_i = 5{\cdot}4$. This value, which is independent of Reynolds number and Prandtl number is predicted accurately for three Reynolds numbers.

The data for other values of y demonstrate that at constant Reynolds number the Nusselt number increases as y decreases. This increase is particularly appreciable at high Reynolds numbers. At low Reynolds numbers, however, the Nu_i data, like the Nusselt number is dependent on both Reynolds number and Prandtl number. The predictions are similar in trend to those found in the case of flow in a curved pipe (see Akiyama and Cheng [14]) where the secondary flow induced by the curvature increases the convective heat transfer.

The important difference between the results for curved pipe and the present predictions is that the increase in the Nusselt number in the Prandtl number range 10–100 is greater than that in the range 1–10. This increase in Nusselt number increases with increase in the Reynolds number. This is because, added to the convection due to secondary velocities (which are large in the twisted tape flow), there is convection due to the component of the axial velocity [i.e. $(\pi/H)V_z$, see equation (8)] which is large at high Reynolds numbers. The substantial increases in Nusselt number obtained at high Prandtl numbers are therefore to be expected.

Also within the range of Re_i and Pr considered here at any fixed Reynolds number, the value of Nu_i/Pr decreases with increase in Pr; showing thus that Nusselt number becomes bounded with increasing Prandtl numbers.

Effect of fin-parameter on Nusselt number—Figure 7 shows the predicted values of Nu_i at $y = 2{\cdot}25$ and ∞ are shown for three values of C_{fin}: 0 (i.e. minimum fin-effect), and 1·85 (i.e. an intermediate fin-effect), and ∞ (i.e. maximum fin-effect). The values of Nu_i for $y = \infty$ represented by the solid lines corresponding to $C_{\text{fin}} = 0$, 1·85, and ∞ are respectively 2·594, 3·801 and 5·4. These values were found to be independent of Re_i and Pr.

Note that the ratio $Nu_{i,\infty}/Nu_{i,0}$ for $y = \infty$ is 2·07. This can be explained as being primarily due to the increase in the surface area available for heat transfer when $C_{\text{fin}} = \infty$ compared to when $C_{\text{fin}} = 0$. Thus, if the average heat-transfer coefficients on the tube wall were identical for $C_{\text{fin}} = 0$ and ∞, and if these coefficients equalled the average heat-transfer coefficient on the tape surface when $C_{\text{fin}} = \infty$, then one could obtain that $Nu_{i,\infty}/Nu_{i,0} = (\pi D + 2D)/\pi D = 1{\cdot}64$. In the present computations the ratio is found to be 2·07 mainly because the average heat-transfer coefficient on the tape surface was greater than that on the tube wall for $C_{\text{fin}} = \infty$; the latter coefficient also being slightly larger than the average coefficient for $C_{\text{fin}} = 0$.

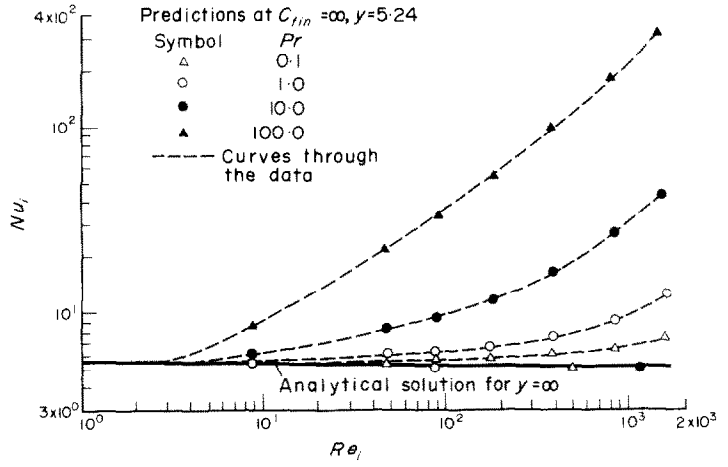

FIG. 6. Influence of Prandtl number on Nusselt number at $C_{\text{fin}} = \infty$.

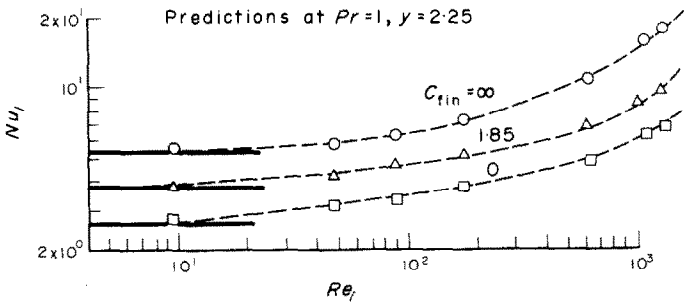

FIG. 7. Influence of fin-parameter on Nusselt number at $y = 2{\cdot}25$. Horizontal lines correspond to $y = \infty$. Dashed lines are curves through the predicted data.

The plausibility of the data for $y = 2{\cdot}25$ is, of course, shown by their asymptotic behaviour at low Reynolds numbers. However, from the designer's point of view, the important observation to be made concerns the values of $Nu_{i,\infty}/Nu_{i,0}$. The value of this ratio is nearly 2·1 at low Reynolds number, whereas at $Re_i = 10^3$, the value of the ratio equals 2·62. Thus, the improvement in heat transfer available from the fin-effect depends on the value of Reynolds number when $y < \infty$; in Date [19], it is shown that it also depends on the value of the Prandtl number.

In Date [19], where many more predicted data are

presented, it is shown that for all practical purposes, a single parameter Re_i/y can be used to correlate the Nu_i data for a particular value of Pr and C_{fin}.

Figure 8 shows typical temperature profiles at $C_{fin} = 0$, 1·85 and ∞. The figure shows that as C_{fin} increases, the difference between the value of the bulk fluid temperature and the tube wall temperature decreases. This supports the trend observed earlier that the Nusselt number, which is inversely proportional to this temperature difference, must increase as the fin-parameter increases. Note also the manner in which the value of C_{fin} affects the gradient of temperature near the tape wall.

4.2.2. *Friction characteristics.* A typical comparison of the predicted friction factor with the available experimental data is shown in Fig. 9 for $y = 4{\cdot}14$. The experimental data are under-predicted by nearly 30 per cent. In Date [19] where comparisons for other values of y are presented, underprediction of the same order of magnitude is observed. While qualitative trends of the predictions is in agreement with the experimental data, their quantitative disagreement is certainly due to the inadequacy of the model of turbulence used in the predictions. The main reason for underprediction is that the value of μ_{eff}, as predicted from k and ε equations, is too small. Com-

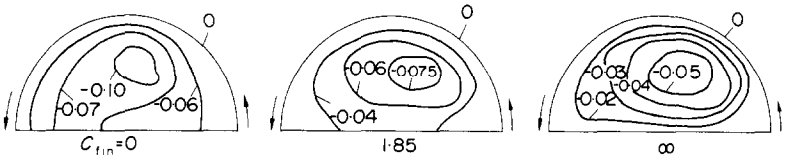

FIG. 8. Influence of the fin-parameter on predicted profiles to T^* at $Re_i = 810$, $y = 5{\cdot}24$ and $Pr = 1{\cdot}0$ (arrows indicate rotation of tape in the direction of flow).

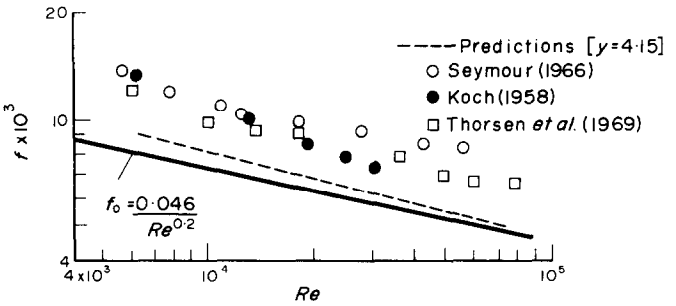

FIG. 9. Comparison of predicted and experimental friction factors.

This completes the presentation and the discussion of the laminar flow characteristics. We now turn to the turbulent flow characteristics.

4.2. *Turbulent flow*

4.2.1. *Method of presentation.* The method employed for prediction of friction and heat-transfer characteristics of the turbulent flow is similar to that described for laminar flow, except that the equations for k and ε are solved with values of C_μ, C_G, C_D, $Pr_{eff.k}$, $Pr_{eff.\varepsilon}$ and $Pr_{eff.T}$ being specified as explained in Section 2. The values of f_i, Re_i and Nu_i are calculated in the same manner as described in Section 4.1, but here these values are divided by the ratio of internal to hydraulic diameters (i.e. D/D_h). This is done to make a meaningful comparison of the predictions with the available experimental data. The value of D/D_h used is 1·66. The friction factor, Reynolds number and Nusselt number thus calculated are referred to by f, Re and Nu respectively.

putational experiments showed that the predictions can be forced to match the experimental data by augmenting the effective viscosity (or C_μ) in the axial velocity equation* by a factor greater than 1. Over the range of Reynolds numbers considered, the value of this factor, however, depended on the value of y. For instance, at $y = 11{\cdot}0$ the value of the augmentation factor was found to be 1·1; at $y = 5{\cdot}15$ to be 1·2; at $y = 4{\cdot}14$ to be 1·35; and at $y = 3{\cdot}14$ to be 1·6. This means that the constant C_μ is not universal, or simply that the turbulent viscosity is not isotropic. Lilley and Chigier [15] have provided experimental evidence to the effect that, in axisymmetric swirling flows, turbulent viscosity must be non-isotropic. Roberts [16], who predicted a decaying swirling flow, could obtain reason-

*The predictions can also be forced to match the experimental data by augmenting the effective viscosity in the vorticity equation.

able predictions only when the turbulent viscosities in the axial and tangential directions were ascribed different values. The turbulent viscosity has directional properties (or is non-isotropic) in these cases, because appreciable velocity gradients (or strains) exist in more than one direction. In the twisted-tape flow, which is non-axisymmetric swirling-type, a similar situation exists.

If such flow situations are to be predicted without *ad hoc* means such as the "augmentation factor" introduced above, then one must do away with the turbulent viscosity concept. Instead, description of the turbulent longitudinal-strains. Account of this fact, the author believes, will bring about the further augmentation of the implied turbulent viscosities to enable quantitatively correct prediction of the friction factor. The computational effort involved, especially in terms of obtaining convergent solutions to the equations cannot be undermined; and it may be more expedient to follow the concept of "augmentation factor" mentioned in the last paragraph.

Figure 10 shows the comparison of the predicted and experimental (Backshall [17]) profiles of axial velocity at $y = 3{\cdot}08$ and $Re_i = 5 \times 10^4$. The agreement between

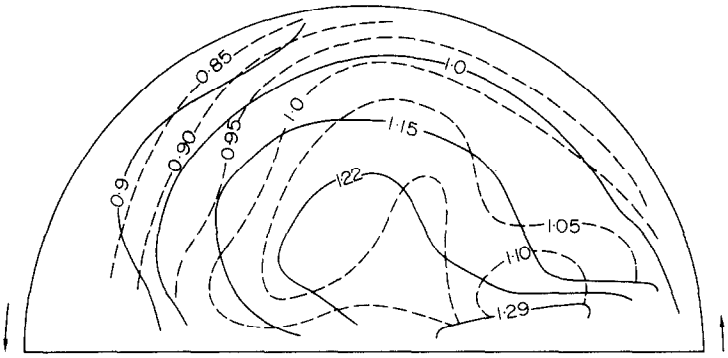

FIG. 10. Comparison of predicted (——) and experimental (– – – –, Backshall [17]) axial velocity profiles ($V_z/V_{z,m}$) at $y = 3{\cdot}08$. (Arrows indicate rotation of tape in the direction of flow.)

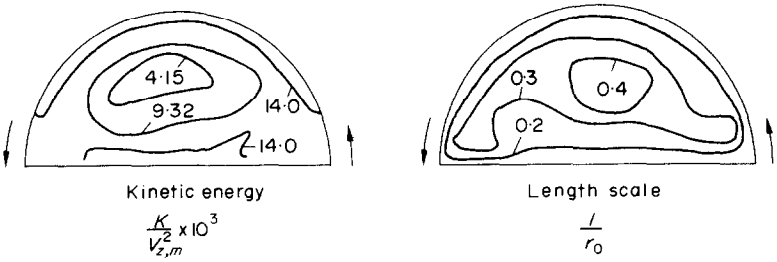

FIG. 11. Predicted profiles of length scale and kinetic-energy at $y = 4{\cdot}15$ and $Re_i = 1{\cdot}2 \times 10^4$. (Arrows indicate rotation of tape in the direction of flow.)

stresses must be obtained from the solution of Reynolds stress equations. The task of this approach is, however, quite formidable at the present time. In Date [19] simplified forms of the Reynolds stress equations are used for prediction purposes. These predictions, although nearly 15 per cent better than the ones described here, do not agree with data. The predicted stresses, however, are such that they indeed imply much larger turbulent viscosities than the ones predicted by solving k and ε equations.

Following Hanjalic' and Launder [23] and Launder and Ying [24], the simplified forms used in Date [19] can be further refined to account for the fact that the stresses in the plane of cross-section are produced by the two profiles is qualitatively acceptable, although the magnitude of the predicted axial velocity in the centre of the cross-section exceeds the measured value by nearly 14 per cent.

Figure 11 shows the typical distributions of the predicted length scale and kinetic energy profiles. The kinetic energy profile is plausible; for near the wall, where the shear stress is maximum, so is the value of energy; near the centre of the cross-section the value of energy diminishes since the shear stress diminishes.

The profiles of the length scale clearly indicate the usefulness of solving the dissipation (ε) equation; for such a length scale distribution, if indeed true, would be difficult to specify algebraically. The predicted dis-

tribution, however, seems plausible; for, as would be expected, the length scale increases as distance from the wall.

The heat-transfer characteristics are examined next.

4.2.3. *Heat-transfer characteristics.* The comparison of the predicted and experimental Nusselt numbers is shown in Fig. 12. The scatter in the experimental data is primarily due to the different fin-effects existing in different experimental set-ups. The predictions were therefore obtained for $C_{fin} = 0$ and ∞; the measured Nusselt number data should lie between these two extremes of the fin-effect. The exact values of the fin-effect for the experimental data are unknown; the investigators expect the fin-effect to be not greater than 10 per cent. This means that the measured Nusselt numbers cannot be more than 10 per cent greater than those for $C_{fin} = 0$.

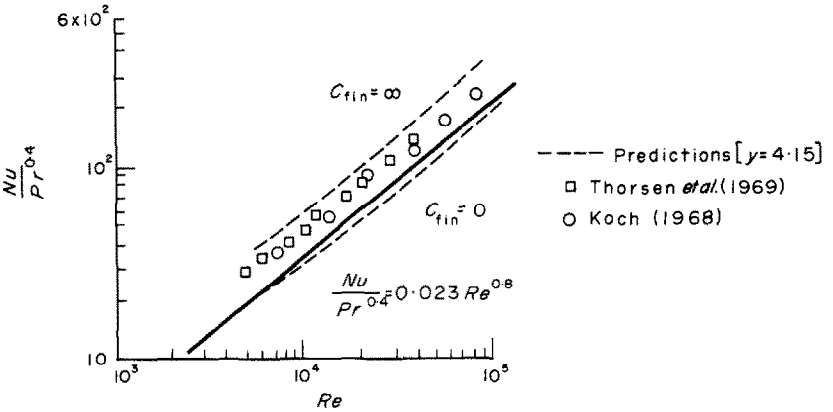

FIG. 12. Comparison of predicted and experimental Nusselt numbers.

That the experimental data lie much closer to the line for $C_{fin} = \infty$ suggests that the Nusselt number data, like the friction factor data, are under-predicted. In Date [19], it is shown that this under-prediction is a direct consequence of the fact that the low magnitudes of the effective viscosity have been predicted. It is important to note, however, that the qualitative trend of the predictions is in agreement with the experimental data, and one can reasonably argue that if the friction factor data were predicted correctly, then so will be the Nusselt number data. Indeed when the augmented turbulent viscosities were used, the Nusselt number predictions were more realistic.

5. CONCLUSIONS

The following are the conclusions of the present paper:

1. The transport equations of the twisted-tape flow are strongly coupled; therefore, the iteration scheme suggested by Gosman *et al.* [6] cannot be employed successfully over the entire range of twist-ratios and Reynolds numbers of interest. The multi-point circulation adjustment procedure must be incorporated in the procedure of Gosman *et al.* to ensure convergence of the solutions.

2. The laminar flow predictions for tapes of finite twist have agreed asymptotically with the analytical solutions for the case of flow in a straight semi-circular duct. The predictions have shown that significant augmentation in heat transfer can be obtained at high Reynolds numbers, high Prandtl numbers, low twist-ratios (i.e. high twists), and high fin-parameters.

3. By solving the differential equations for kinetic energy and its dissipation rate, the need for algebraic specification of the effective viscosity or of the length-scale has been removed.

4. The constants in the turbulence model, as suggested by Jones and Launder [10], although quite universal for flows in which velocity gradients are appreciable only in one direction, are found to be inadequate for predicting the twisted-tape flow characteristics. The constants, for example, under-predict the value of the friction factor (and consequently the Nusselt number). Qualitatively, however, the constants predict data which are in agreement with the experimental data.

5. The quantitative disagreements, mentioned above, expose the inadequacy of the effective-viscosity concept in modelling turbulent stresses in twisted-tape flow. Future research must seek to obtain the information regarding the stresses from the Reynolds stress equations.

Acknowledgements—The author is grateful to Professor D. B. Spalding for suggesting the rotating coordinate system which forms the basis of the present work. The author is also grateful to Dr J. H. Whitelaw who read the first draft of this paper and made suggestions for improvement.

The work reported in the paper was carried out as a part of the author's Ph.D. research programme; the financial assistance provided by the Science Research Council is gratefully acknowledged.

REFERENCES

1. E. Smithberg and F. Landis, Friction and forced convection heat-transfer characteristics in tubes with twisted tape swirl generators, *J. Heat Transfer* **86**, 39–49 (1964).
2. R. Thorsen and F. Landis, Friction and heat-transfer characteristics in turbulent swirl flow subjected to large transverse temperature gradients, *J. Heat Transfer* **90**, 87–97 (1968).
3. R. F. Lopina and A. E. Bergles, Heat transfer and pressure-drop in tape generated swirl flow, M.I.T., Dept. of Mech. Engng, Rep. No. DSR 70281-47 (1967).
4. R. B. Bird, W. E. Stewart and E. N. Lightfoot, *Transport Phenomena*. John Wiley, New York (1960).
5. D. B. Spalding, Contribution to the theory of heat transfer across a turbulent boundary layer, *Int. J. Heat Mass Transfer* **7**, 743–761 (1964).
6. A. D. Gosman, W. M. Pun, A. K. Runchal, D. B. Spalding and M. Wolfstein, *Heat and Mass Transfer in Recirculating Flows*. Academic Press, London (1969).
7. A. D. Gosman and D. B. Spalding, Computation of laminar flow between shrouded rotating discs, Imperial College, Mech. Eng. Dept., Rep. No. EF/TN/A/30 (1970).
8. A. N. Kolmogorov, Equations of turbulent motion in incompressible fluid, *Izv. Akad. Nauk. SSSR, Series Fiz.* **6**, 56 (1942). Also Imperial College, Mech. Eng. Dept., Rep. No. N/6 (1968).
9. L. Prandtl, Über ein neues Formelsystem der ausgebildeten Turbulenz, Nachr. Akad. Wiss. Gottingen, Math-Phys. KL, p. 6 (1945).
10. W. P. Jones and B. E. Launder, The prediction of laminarization with a two-equation model of turbulence, *Int. J. Heat Mass Transfer* **15**(2), 301–314 (1972).
11. L. Mathews, Performance of some two-dimensional film cooling geometries, Ph.D. Thesis, University of London (1972).
12. A. Weigand, The problem of torsion in prismatic members of circular segmental cross-section, NACA Tech. Memo., No. 1182, translation of the original German paper in *Luftfahrt Forschung* **20**(12), 333–340 (1944).
13. E. R. G. Eckert, T. F. Irvine, Jr. and J. T. Yen, Local laminar heat transfer in wedge-shaped passages, *Trans. Am. Soc. Mech. Engrs* **80**, 1433–1438 (1958).
14. M. Akiyama and K. C. Cheng, Boundary vorticity method for laminar flow forced convection heat transfer in curved pipes, *Int. J. Heat Mass Transfer* **14**, 1659–1675 (1971).
15. D. G. Lilley and N. A. Chigier, Non-isotropic turbulent stress distribution in swirling flows from mean value distributions, *Int. J. Heat Mass Transfer* **14**(4), 573 (1971).
16. L. W. Roberts, Turbulent swirling flows with recirculation, Ph.D. Thesis, University of London (1972).
17. R. G. Backshall and F. Landis, The boundary layer velocity distribution in turbulent swirling pipe flow, *J. Bas. Engng* **91**, 728–733 (1969).
18. A. W. Date, Review of single-phase forced convection data for flow in tubes containing twisted-tapes, *Heating & Ventilating Engr J. Air Conditioning* (November 1973).
19. A. W. Date, Prediction of friction and heat transfer characteristics of a flow in a tube containing a twisted-tape, Rep. No. HTS/73/15, Dept. of Mech. Engng, Imperial College (1972).
20. J. Laufer, The structure of turbulence in fully-developed pipe flow, NACA, Rep. No. 1174 (1954).
21. E. V. Seymour, Fluid flow through tubes containing twisted tapes, *The Engineer* **222**, No. 5779 (1966).
22. R. Koch, Pressure loss and heat transfer for turbulent flow, *ForschHft. Ver. Dt. Ing.* **24**, Series 13, No. 469, 144 (1958). English translation AEC-tr-3875.
23. K. Hanjalic' and B. E. Launder, A Reynolds stress model of turbulence and its application to asymmetric boundary layers, Imperial College, Mech. Engng Dept., TM/TN/A/8 (1971).
24. B. E. Launder and W. M. Ying, Fully-developed turbulent flow in ducts of square cross-section, Imperial College, Mech. Engng Dept., Rep. No. TM/TN/A/11 (1971).
25. D. B. Spalding and C. L. V. Jayatillake, A survey of the theoretical and experimental information on the resistance of laminar sub-layer to heat and mass transfer, Proc. 2nd All Soviet Union Conference on Heat and Mass Transfer, Minsk, U.S.S.R. (1966).
26. S. V. Patankar and D. B. Spalding, *Heat and Mass Transfer in Boundary Layers*. Morgan-Grampian, London (1967).

PREVISION DE L'ECOULEMENT ETABLI DANS UN TUBE CONTENANT UN RUBAN HELICOÏDAL

Résumé—On formule par les équations aux dérivées partielles du mouvement et du transfert thermique, l'écoulement établi laminaire ou turbulent d'un fluide à propriétés constantes, dans un tube contenant un ruban hélicoïdal. Ces équations sont résolues en adaptant une méthode numérique déjà existante pour les équations elliptiques bidimensionnelles. On calcule les caractéristiques de frottement et de transfert thermique.

On présente un ensemble de calculs pour l'écoulement laminaire de façon à montrer l'influence du nombre de Reynolds, du pas de l'hélice, du nombre de Prandtl et du paramètre d'ailette.

Pour calculer la viscosité turbulente nécessaire, on résout les équations aux dérivées partielles de l'énergie cinétique turbulente et du taux d'énergie dissipée. Cette approche est néanmoins insuffisante pour des prévisions quantitative exactes; on suggère une modification pour éliminer cette imperfection.

BERECHNUNG EINER AUSGEBILDETEN STRÖMUNG IN EINEM ROHR MIT SPIRALEINBAUTEN

Zusammenfassung—Für den Fall ausgebildeter laminarer und turbulenter Strömung mit einheitlichen Stoffeigenschaften in Rohren mit eingebauten Spiralen wurden partielle Differentialgleichungen für Impuls- und Wärmeaustausch aufgestellt.

Um Druckabfall und Wärmeübergang der Strömung zu berechnen, wurden die Gleichungen durch Anpassung einer bekannten numerischen Prozedur für zweidimensionale elliptische Funktionen gelöst. Die Ergebnisse für laminare Strömung sind wiedergegeben, um den Einfluß der *Re*-Zahl, des Windungsverhältnisses, der *Pr*-Zahl und des Rippenparameters auf die Strömungsform zu zeigen. Die scheinbare Zähigkeit, die man braucht, um die Eigenschaften der turbulenten Strömung zu bestimmen, wurde berechnet aus der Differentialgleichung für die kinetische Energie der Turbulenz und die Größe der Dissipationsenergie. Es zeigte sich, daß diese Näherung für genaue quantitative Aussagen nicht ausreicht. Es wird ein Verbesserungsvorschlag gemacht.

РАСЧЕТ ПОЛНОСТЬЮ РАЗВИТОГО ПОТОКА В ТРУБЕ СО ШНЕКОМ

Аннотация — Задача о полностью развитом ламинарном и турбулентном однородном течении в трубе со шнеком сформулирована с помощью уравнений переноса импульса и тепла в частных производных. Эти уравнения решены путем модификации метода, применяемого в двумерных эллиптических уравнениях, для расчета коэффициентов трения и теплообмена потока.

Приведенные расчетные данные для ламинарного течения показывают влияние числа Рейнольдса, коэффициента закручивания, числа Прандтля и параметра ребра на характеристики потока.

Коэффициент турбулентной вязкости, необходимый для расчета характеристик турбулентного течения, рассчитывался путем решения дифференциальных уравнений кинетической энергии турбулентности и скорости диссипации энергии. Однако, установлено, что такой метод оказался непригодным для точных количественных расчетов. Предлагается способ устранения этого недостатка.